COVER SHEET

This is the author version of a paper published as:

Schultz, Madeleine and Sofield, Chadwick D. and Walter, Marc D. and Andersen, Richard A. (2005) Coordination complexes of bivalent ansa-ytterbocenes: synthesis, structure and comparison with related unbridged ytterbocenes and ansa-ferrocenes. New Journal of Chemistry 29:pp. 919-927.

Accessed from http://eprints.qut.edu.au

Copyright 2005 Royal Society of Chemistry

CREATED USING THE RSC ARTICLE TEMPLATE - SEE WWW.RSC.ORG/ELECTRONICFILES FOR FURTHER DETAILS

Coordination Complexes of Bivalent *ansa*-Ytterbocenes: Synthesis, Structure and Comparison with Related Unbridged Ytterbocenes and *ansa*-Ferrocenes

Madeleine Schultz, Chadwick D. Sofield, Marc D. Walter and Richard A. Andersen*

Chemistry Department and Chemical Sciences Division of Lawrence Berkeley National Laboratory, University of California, Berkeley, California 94720, USA. Fax: 1 510 486 5596; Tel: 1 510 642 4452; E-mail: raandersen@lbl.gov

***This submission was created using the RSC Article Template* (*DO NOT DELETE THIS TEXT*)**
(*LINE INCLUDED FOR SPACING ONLY - DO NOT DELETE THIS TEXT*)

The dimethylsilyl bridged bis(cyclopentadienide) ligands, $\{[2,4\text{-}(Me_3C)_2C_5H_2]_2SiMe_2\}^{2-}$ and $\{[(Me_3Si)_2C_5H_2]_2SiMe_2\}^{2-}$, have been prepared and used for the preparation of *ansa*-metallocene derivatives of iron and bivalent ytterbium metallocene adducts. The structures of two *ansa*-ferrocenes, as well as that of the free tetraene $[2,4\text{-}(Me_3C)_2C_5H_3]_2SiMe_2$, have been determined by X-ray crystallography, and the lability of the Me_3Si group leads to a different ring substitution pattern in the structure of *ansa*-$\{[3,4\text{-}(Me_3Si)_2C_5H_2]_2SiMe_2\}Fe$ compared with that in *ansa*-$\{[2,4\text{-}(Me_3C)_2C_5H_2]_2SiMe_2\}Fe$. The structures of *ansa*-$\{[2,4\text{-}(Me_3C)_2C_5H_2]_2SiMe_2\}Yb(OEt_2)$ and an analogous *ansa*-ytterbocene isocyanide complex are also reported, and compared with those of non-bridged ytterbocene diethyl ether complexes. Short distances from the ytterbium atom to the diethyl ether β carbon atoms are observed in several structures, consistent with the tendency of ytterbium to maximise its coordination number. Spectroscopic properties for the *ansa*-ytterbocene etherates and the isocyanide complex are reported and compared with the corresponding adducts of non-bridged ytterbocenes. The reduced Cp(centroid) - metal - Cp(centroid) angle enforced by the *ansa*-bridge does not lead to significant changes in the optical spectra compared with unbridged metallocene diethyl ether and tetrahydrofuran adducts, but significant changes are observed in the isocyanide adducts; a model rationalising the red and blue shifts of λ_{max} is proposed.

Introduction

The design and use of "*ansa*-cyclopentadienyl" ligands to direct and control the stereochemistry at metal centres in polymerisation and other catalytic reactions is a commercial development of great importance.[1, 2] This development has largely been concentrated on the group 4 metals in general and on zirconium cations in particular, but the neutral group 3 metals and lanthanides have also been studied in this context.[3, 4] Although many trivalent lanthanide *ansa*-metallocenes have been prepared and their potential as catalysts for several transformations has been explored,[5] only a few *ansa*-metallocenes have been described for the bivalent lanthanides; several are based on Sm(II)[6] and only two on Yb(II).[7, 8] The samarium(II) *ansa*-metallocene, $\{[2,4\text{-}(Me_3Si)_2C_5H_2][3,4\text{-}(Me_3Si)_2C_5H_2]SiMe_2\}Sm(THF)_2$, with C_1 symmetry, has been obtained from the reaction of the dipotassium salt of the ligand, generated by deprotonation of the tetraene $[(Me_3Si)_2C_5H_3]_2SiMe_2$ with ^nBuLi and KO^tBu, with SmI_2 in THF.[6] When the bridge is Ph_2Si rather than Me_2Si, the C_{2v} symmetry samarocene, *ansa*-$\{[3,4\text{-}(Me_3Si)_2C_5H_2]_2SiPh_2\}Sm(THF)_2$, was obtained;[6] thus, the regiochemistry depends upon the barrier for the silatropic shifts of the silyl substituents.

The Lewis acidity of base-free ytterbocenes, specifically $(Me_5C_5)_2Yb$, has been studied in order to develop a bond model for weak metal to ligand bonding when the Lewis base is, for example, CO.[9-12] A feature of the model is that as the Cp(centroid)-M-Cp(centroid) angle gets smaller the developing dipole moment, with the positive end located on the metal centre, gets larger, increasing the electrostatic interaction between the metal fragment and the ligand dipole, so the bond becomes stronger. Since the Cp(centroid)-M-Cp(centroid) angle in an *ansa*-metallocene is smaller than in an unbridged metallocene, an *ansa*-ytterbocene became a synthetic target. In this paper we describe synthetic, X-ray crystallographic and spectroscopic data of several adducts *ansa*-$\{[2,4\text{-}(Me_3C)_2C_5H_2]_2SiMe_2\}Yb(L)$, as well as the ligand synthesis and related ferrocene complexes, which were prepared in order to confirm the connectivity of the *ansa* ligand. The optical spectra of the diethyl ether and THF adducts of the bridged and some of the unbridged ytterbocenes were studied and compared with the molecular structures of the diethyl ether adducts of *ansa*-$\{[2,4\text{-}(Me_3C)_2C_5H_2]_2SiMe_2\}Yb$, $(Me_5C_5)_2Yb$ and $[1,3\text{-}(Me_3C)_2C_5H_3]_2Yb$, determined by X-ray crystallography, in order to rationalise how the colours change as a function of bend angle.

Results and Discussion

Synthesis and Structures

Ligands and Ferrocenes

The tetraene, $[(Me_3Si)_2C_5H_3]_2SiMe_2$, was obtained as a mixture of isomers by the magnesocene route and the mixture was converted to the *ansa*-magnesocene, which was then allowed to react with $FeBr_2(THF)_2$ in THF, as described in the Experimental Section. A single isomer of the ferrocene, *ansa*-$\{[3,4\text{-}(Me_3Si)_2C_5H_2]_2SiMe_2\}Fe$, was isolated in low yield by crystallisation from hexane as large red-purple crystals. This sequence of synthetic reactions that lead to the synthesis and structure of the ansa-ferrocene was developed as a structural proof of the synthetic methodology. An ORTEP diagram is shown in Figure 1 and important bond distances and angles are in Table 1; data collection and structure solution parameters are in Table 2.

Inspection of the structure shows that the idealised symmetry is C_s and therefore the *meso* isomer crystallised. The ^1H NMR spectrum in C_6D_6 is consistent with the crystallographic result, see Experimental Section for details. As can be seen from Figure 1, the $SiMe_2$ bridge enforces an eclipsed geometry of the two cyclopentadienyl rings, and the *meso* configuration forces the substituents to be eclipsed as well, in what appears to be a sterically demanding arrangement.

The Me_3C analogue of the Me_3Si derivative has been used to prepare the zirconocene dichloride and dicarbonyl derivatives, but no synthetic details have been published.[13, 14] We have prepared the tetraene, $[2,4\text{-}(Me_3C)_2C_5H_3]_2SiMe_2$, by the magnesocene route, see Experimental Section for details. This

tetraene is obtained as colourless crystals from hexane and the structure was determined by X-ray crystallography; an ORTEP diagram is shown in Figure 2 with important structural parameters listed in the figure caption, while data collection and structure solution parameters are given in Table 2.

The ^{1}H NMR spectrum of this molecule in C_6D_6 at 25 °C shows only one isomer to be present in solution and the structure shows it to be the isomer in which the Me_3C groups are in the 2- and 4-positions in both rings. The tetraene was converted to the magnesocene and then to the ferrocene, *ansa*-{[2,4-$(Me_3C)_2C_5H_3]_2SiMe_2$}Fe, as a structural proof. The ferrocene crystallises from hexane as red crystals whose solid state structure is shown in Figure 3; bond lengths and angles are listed in Table 1 and data collection and structure solution parameters are included in Table 2.

The structure has idealised C_2 symmetry and therefore the *rac* isomer crystallised; in contrast to the Me_3Si derivative, the enforced eclipsed conformation of the Cp rings now results in the ring substituents lying between each other, in what appears a less sterically demanding configuration. The ^{1}H NMR spectrum is consistent with C_2 symmetry in C_6D_6 solution. Isolation of the *meso*-ferrocene isomer when the substituents are Me_3Si and the *rac*-ferrocene isomer when the substituents are Me_3C presumably is related to the lower barrier for Me_3Si fluxional motion relative to Me_3C shifts in neutral and anionic cyclopentadienyl compounds.[15]

Ytterbocenes

The *ansa*-magnesocenes are not useful as synthons for the ytterbocenes because they do not react with YbI_2 in diethyl ether, or under any other conditions examined. However, the disodium salt of the Me_3C tetraene, obtained by reaction of the tetraene with $NaNH_2$, is a useful synthon. Thus, the diethyl ether complex *ansa*-{[2,4-$(Me_3C)_2C_5H_2]_2SiMe_2$}$Yb(OEt_2)$ can be synthesised by reaction of the sodium salt of the substituted cyclopentadienide with ytterbous iodide in diethyl ether, followed by filtration and crystallisation from the deep green mother liquor (Equation 1).

$$Na_2Cp'_2 + YbI_2 \rightarrow Cp'_2Yb(OEt_2) + 2NaI \quad (1)$$

Cp'_2 = {[2,4-$(Me_3C)_2C_5H_2]_2SiMe_2$}$^{2-}$

It is important that the THF-free reagent is used, otherwise a mixture of the diethyl ether and THF complexes will result. The latter is due to residual THF bound to the sodium salt of the ligand, which can be removed by prolonged exposure of the powdered sodium salt to dynamic vacuum. Preparation of the pure THF complex results from the reaction described in equation 1, when THF is used as solvent.

The etherate *ansa*-{[2,4-$(Me_3C)_2C_5H_2]_2SiMe_2$}$Yb(OEt_2)$ cannot be desolvated by any of the published methods used to prepare base-free ytterbocenes.[16] Attempted sublimation leads to an insoluble brown solid, as does the toluene reflux method. The tetraene does not react with $Yb[N(SiMe_3)_2]_2$ in toluene.

The structure of the diethyl ether complex, *ansa*-{[2,4-$(Me_3C)_2C_5H_2]_2SiMe_2$}$Yb(OEt_2)$, was determined for comparison with the known structures of $(Me_5C_5)_2Yb(OEt_2)$[17] and [1,3-$(Me_3C)_2C_5H_3]_2Yb(OEt_2)$.[18] A room temperature structure of the latter has been reported, but the low temperature data set collected in this work will be used for comparison as it was obtained under identical conditions to the other structures described here. The published structure is slightly different from that determined in this work, but the space group is the same and the important bond distances and angles are within 1% of those described here. Table 3 contains important bond distances and angles for the three structures, Table 4 contains important data collection and structure solution parameters, while Figures 4 and 5 show ORTEP diagrams of the diethyl ether complexes.

The structures of the diethyl ether complexes involve typical Yb(II) bond distances to the cyclopentadienyl ligands in 7-coordination.[19] The geometries about the metal centre are not surprising, and the most interesting feature in these structures is the disposition of the diethyl ether ligand. In $(Me_5C_5)_2Yb(OEt_2)$, one of the γ-Me groups of the ether ligand is bent back towards the metal centre,[17] with an ytterbium ··· carbon distance of 3.23(1) Å, which is significantly shorter than the sum of the van der Waals radii of a methyl group (2.00 Å) and the metallic radius of Yb(II) (1.70 Å).[20] This type of interaction is typical of lanthanide complexes, which generally display the highest possible coordination number without causing undue steric congestion.[16] The complex *ansa*-{[2,4-$(Me_3C)_2C_5H_2]_2SiMe_2$}$Yb(OEt_2)$ crystallises with three unique molecules in the asymmetric unit; one of which is shown in Figure 4. Each of these molecules has one short Yb ··· γ-Me distance; in molecule 1, Yb(1) ··· C(29) is 3.14 Å; in molecule 2 and molecule 3 the equivalent distances are 3.15 Å, and 3.00 Å, respectively. These distances are only about 10 % longer than the longest ring carbon - ytterbium distances observed in typical Yb(II) metallocenes.[16, 21-26] The ytterbium atom is exposed to this interaction because of the *ansa*-bridge, which holds the metallocene wedge open with a Cp(centroid)-Yb-Cp(centroid) angle of 124°, and allows the close approach of the γ-Me groups of the ether ligand without undue steric congestion between the ligands.

In the structure of [1,3-$(Me_3C)_2C_5H_3]_2Yb(OEt_2)$, the ether ligand is twisted so that both γ-Me groups of the ligand point away from the metal (Figure 5). The Cp(centroid)-Yb-Cp(centroid) angle of 132° in [1,3-$(Me_3C)_2C_5H_3]_2Yb(OEt_2)$ is 8° smaller than in $(Me_5C_5)_2Yb(OEt_2)$, suggesting that the Cp rings can rotate out of each others' way in order to bend more than in the pentamethylcyclopentadienide analogue, which is less flexible. However, the bulky Me_3C groups at the front of the wedge presumably prevent the close approach of the γ-Me groups of the ether ligand. While no non-bonded metal ··· carbon distance of less than 3.5 Å is observed in this structure, two of the methyl carbon atoms of the Me_3C groups approach the metal within the sum of the van der Waals radii; the Yb ··· C(13) distance is 3.67 Å and the Yb ··· C(24) distance is 3.59 Å. These two carbon atoms are located at the same side of the wedge, one on each cyclopentadienide ring. Similar intramolecular interactions are observed in the solid state structure of the base-free analogue [1,3-$(Me_3C)_2C_5H_3]_2Yb$, in contrast to other base-free ytterbocenes, which crystallise with short intermolecular Yb - C distances.[16]

The diethyl ether structures provide evidence that any available interaction will occur to reduce coordinative unsaturation in a bivalent ytterbocene. There is not enough room within the coordination sphere for a second diethyl ether ligand, so the Yb ··· γ-Me interaction occurs. The various conformations of the ethyl groups in the diethyl ether adducts in the solid state are also consistent with the idea that the specific conformations are energetically similar and the observed conformation is the one that minimises all repulsive interactions while maximizing the attractive ones.[16]

The xylyl isocyanide complex of *ansa*-{[2,4-$(Me_3C)_2C_5H_2]_2SiMe_2$}Yb can be prepared from either the diethyl ether adduct or the THF adduct by stirring the ytterbocene with the isocyanide in toluene. The resulting 1:2 adduct is relatively insoluble in aromatic and aliphatic solvents and can be crystallised from toluene as dark red blocks. The infrared spectrum of the isocyanide complex contains a band at 2127 cm^{-1} for the CN stretch, which is 9 cm^{-1} higher than the free

isocyanide. The single, sharp CN stretch in both the solid state and toluene solution is in accord with those previously described for 1:2 complexes of unbridged ytterbocenes.[9] The structure of the *ansa*-ytterbocene isocyanide complex was determined for comparison with the published ytterbocene isocyanide complexes.[9] Figure 6 shows an ORTEP diagram, and important bond distances and angles are presented in Table 3 and the figure caption, while data collection and structure solution parameters are included in Table 4. The structure exhibits the expected reduction in Cp(centroid)-Yb-Cp(centroid) angle due to the *ansa*-bridge. The arrangement of the xylyl isocyanide ligands is not affected, however; the averaged Yb-C(isocyanide) distance of 2.57 Å is slightly shorter than that in [1,3-$(Me_3C)_2C_5H_3]_2$Yb(CN-2,6-$Me_2C_6H_3$) of 2.61 Å, while the angle between the isocyanide ligands is identical.

Optical Spectroscopy

The optical spectra of the diethyl ether and THF complexes of the *ansa*-ytterbocene, along with the other substituted ytterbocenes described here and previously,[16] have been measured and the data are presented in Table 5. The diethyl ether adducts are green in colour, while the colours of the THF complexes vary widely; some are bright green while others are red. These observations can be rationalised according to the Rösch-Green model presented previously[9] as follows.[27]

When a 1:1 or 1:2 adduct of a metallocene forms, the resulting Cp(centroid)-M-Cp(centroid) angle of the bent sandwich is smaller than in the base-free complex. The donor ligands interact with the empty a_1 (a_1 and b_2 in a 1:2 adduct) (C_{2v} symmetry) orbitals of *d*-orbital parentage, generating one or two (in a 1:1 or a 1:2 adduct respectively) bonding orbitals and antibonding ones (Figure 7). The net result of adduct formation is therefore to leave the LUMO orbital largely unaffected. However, the filled orbitals of *f*-parentage including the HOMO are increased somewhat in energy since adding electron density raises their energy. This destabilisation can be thought of as arising from the increased electron - electron repulsion in the *f*-orbitals in the closed shell, $4f^{14}$ Yb(II). This effect is not expected to be large, however, as the nephelauxetic effects for the lanthanides are of similar magnitude as for the *d*-transition metals, and cause a decrease in electron - electron repulsion due to the expanded *f*-orbitals.[28] Thus, the net effect on the HOMO → LUMO transition as a result of adduct formation could be either a blue or a red shift depending on the extent of bending that increases the HOMO - LUMO gap and the extent of electron - electron repulsion that decreases it.

The ytterbocene diethyl ether complexes all have very similar optical spectra, with the long wavelength feature assigned to the HOMO → LUMO transition varying only slightly from 690 nm for $(Me_5C_5)_2$Yb(OEt_2) to 653 nm for [1,3-$(Me_3Si)_2C_5H_3]_2$Yb(OEt_2) (Figure 8). Although the solid state structure of [1,3-$(Me_3Si)_2C_5H_3]_2$Yb(OEt_2) is not known, it is presumably similar to that of [1,3-$(Me_3C)_2C_5H_3]_2$Yb(OEt_2) because their solution optical spectra are the same. It is interesting that the complex $(Me_4C_5H)_2$Yb(OEt_2) exhibits a HOMO → LUMO transition at 683 nm, close to that for the penta-substituted analogue, implying that the bend angles are similar in solution. The *ansa*-bridged complex has a much lower Cp(centroid)-Yb-Cp(centroid) angle in the solid state and presumably in solution also, yet it has a HOMO → LUMO transition that is similar to those of the other ytterbocene - diethyl ether adducts. Presumably the sterically accessible metal centre leads to greater electron - electron repulsion, so the transition is only slightly red-shifted relative to the unbridged disubstituted ytterbocenes. The two high energy transitions are the same for all of the ytterbocene diethyl ether complexes, at 465 and 400 nm, which indicates that the $f \rightarrow d$ and LMCT transitions are insensitive to the ligand environment, as observed in the dipyridyl adducts.[29]

The bond model developed for the diethyl ether adducts may be extended to the isocyanide adduct. As the Cp(centroid)-Yb-Cp(centroid) angle gets smaller, the energy of the LUMO decreases while that of the HOMO increases. Since the Cp(centroid)-Yb-Cp(centroid) angle in the *ansa*-ytterbocene isocyanide is 11° smaller than in [1,3-$(Me_3C)_2C_5H_3]_2$Yb(CNxylyl)$_2$, a red shift is expected and observed; the λ_{max} of the *ansa* derivative is observed at 686 nm (Table 5), while that of the non-bridged analogue is at 586 nm.[9]

The colours and transitions of the THF complexes are less readily explained (Figure 9). The adduct $(Me_5C_5)_2$Yb(THF) crystallises from toluene as bright red crystals with half an equivalent of toluene of crystallisation.[21] However, in THF solvent the molecule is thought to have two equivalents of THF per metal centre, $(Me_5C_5)_2$Yb$(THF)_2$, and a red molecule containing two equivalents of THF, by integration of the ^{1}H NMR spectrum, can be crystallised from pentane solvent. The slightly-less substituted analogue $(Me_4C_5H)_2$Yb$(THF)_2$ crystallises with two equivalents of THF from diethyl ether or THF,[30] and is also red. Crystallisation of $(Me_4C_5H)_2$Yb$(THF)_2$ from toluene yields a molecule that, by integration of the ^{1}H NMR spectrum, contains a single THF molecule per ytterbium atom and is also bright red. In contrast, the molecule [1,3-$(Me_3C)_2C_5H_3]_2$Yb(THF) contains a single THF ligand whether crystallised from diethyl ether or toluene and is green, with an optical spectrum that is not dissimilar from the diethyl ether adduct. The brown Me_3Si analogue also has a single THF ligand, [1,3-$(Me_3Si)_2C_5H_3]_2$Yb(THF).[19] When dissolved in THF, this complex changes colour to bright purple, but an adduct containing more than one equivalent of THF cannot be obtained by crystallisation. Presumably the steric bulk of the disubstituted cyclopentadienide rings leads to the 7- rather than 8-coordinate complexes in the solid state. The sterically less-encumbered, and electronically more exposed *ansa*-{[2,4-$(Me_3C)_2C_5H_2]_2SiMe_2$}Yb$(THF)_2$ crystallises with two equivalents of THF, by integration of the ^{1}H NMR spectrum, as red needles.

Thus, the ytterbocenes with two equivalents of THF are all red, while those with a single THF ligand vary from green to brown to red, depending on the substituents on the cyclopentadienide rings. In the solid state, the bend angle of an ytterbocene complex with two ethereal ligands is no different from that of a complex with only one.[19] It is therefore tempting to suggest that the red colour of the ytterbocenes with two equivalents of THF results from a red-shift in the HOMO → LUMO transition due to increased electron - electron repulsion from the second ligand which raises the energy of the HOMO, while the LUMO is not strongly affected as the bend angle is not changed. However, the optical spectra of the complexes which can be crystallised with either one or two equivalents of THF are identical, regardless of the stoichiometry deduced from the ^{1}H NMR spectra. This suggests that the second THF is not bound to the metal in solution, and exchanges rapidly on the NMR timescale. No molecular structures have been determined crystallographically for these complexes, and the reported structures of ytterbocenes bound to two THF ligands involve less substituted cyclopentadienide rings.[31, 32] Therefore, the differences in colour must result from the balance of electron - electron repulsion with the bend angle of the ytterbocene.

Conclusions

The preparation of a single isomer of an *ansa*-bridged bis(cyclopentadienide) ligand bearing silyl groups is complicated by the lability of the carbon - silicon bond upon deprotonation of

the cyclopentadienide ring. Thus, the two *ansa*-ferrocenes reported here, containing Me_3Si groups and Me_3C groups, have 3,4 and 2,4 substitution patterns respectively, although the synthetic routes used were analogous. The solution and crystallographic characterisation of the free Me_3C-substituted tetraene provides evidence in that case that the ring substitution pattern is unaffected by deprotonation and coordination to iron.

The strength of coordination of diethyl ether in the adduct of the divalent *ansa*-ytterbocene precludes formation of a base-free *ansa*-ytterbocene. As the metallocene bends, the net dipole moment increases, resulting in a larger electrostatic interaction between the dipoles on the Lewis acid and Lewis base compared with an unbridged ytterbocene. This interaction compensates the free energy of dissociation, rendering the ether adduct stable except to exchange with stronger Lewis bases. The additional room available around the metal centre due to the small Cp(centroid)-Yb-Cp(centroid) angle in the *ansa*-ytterbocene is partially occupied in the solid state structure by γ-agostic interactions with the diethyl ether ligand.

The νCN in the infrared spectra of the 2,6-$Me_2C_6H_3NC$ adducts of *ansa*-{[2,4-$(Me_3C)_2C_5H_2]_2SiMe_2$}Yb and [1,3-$(Me_3C)_2C_5H_3]_2$Yb are nearly identical, presumably reflecting the notion that the electron density at the Yb(II) centre in the metallocenes is nearly identical. The long wavelength absorptions, however, differ by 500 cm^{-1} (100 nm), which is a reflection of the smaller bend angle in the bridged metallocene and therefore the extent to which the HOMO - LUMO gap decreases.

Experimental

General

All reactions and product manipulations were carried out under dry nitrogen using standard Schlenk and drybox techniques. Dry, oxygen-free solvents were employed throughout. The elemental analyses and mass spectra were performed at the analytical facility at the University of California at Berkeley. The following compounds were prepared as previously described: [1,3-$(Me_3Si)_2C_5H_3]_2Mg$,[33] [1,3-$(Me_3C)_2C_5H_3]_2Mg$,[34, 35] Br_2SiMe_2,[36] $NaNH_2$,[37] YbI_2,[38] $Yb(N(SiMe_3)_2)_2(OEt_2)_2$,[38] $Yb(N(SiMe_3)_2)_2$,[39] $(Me_5C_5)_2Yb(OEt_2)$,[38] $(Me_5C_5)_2Yb(THF)$,[21] [1,3-$(Me_3Si)_2C_5H_3]_2Yb(OEt_2)$,[26] $(Me_4C_5H)_2Yb(OEt_2)$[16] and [1,3-$(Me_3C)_2C_5H_3]_2Yb(OEt_2)$.[16, 18] $(Me_5C_5)_2Yb(THF)_2$ was prepared by dissolving the mono-THF adduct in THF and crystallising from pentane (integration of the ^{1}H NMR spectrum indicates that it is a bis(THF) adduct). The structure of [1,3-$(Me_3Si)_2C_5H_3]_2Yb(THF)$ has been reported[19] but no further characterisation has been published. The isocyanide 2,6-$Me_2C_6H_3NC$ was purified by sublimation.

Syntheses

[2,4-$(Me_3C)_2C_5H_3]_2SiMe_2$. The complex [1,3-$(Me_3C)_2C_5H_3]_2Mg$ (10.0 g, 26 mmol) was dissolved in THF (50 mL) and cooled to 0°C. Dibromodimethylsilane (3.4 mL, 26 mmol) was added slowly using a syringe. The reaction mixture was allowed to warm to room temperature and was stirred overnight, producing a yellow solution with a colourless precipitate. The solvent was removed under reduced pressure and the residue was extracted with hexane (50 mL). The filtered extract was concentrated to a volume of 15 mL and cooled to -20°C, which yielded colourless crystals over a period of 3 days (5.4 g, 50%). Anal. Calcd for $C_{28}H_{46}Si$: C, 81.47; H, 11.72. Found: C, 81.50; H, 11.88. ^{1}H NMR (C_6D_6): δ 6.69 (s, 4H, C_5H_3), 5.0 (broad s, 2H, C_5H_3), 1.55 (s, 36H, Me_3C), 0.11 (s, 6H, Me_2Si) ppm.

[$(Me_3Si)_2C_5H_3]_2SiMe_2$. A procedure similar to that used to prepare [2,4-$(Me_3C)_2C_5H_3]_2SiMe_2$ was followed (above). The hexane solution was filtered and the solvent was removed under reduced pressure. The product was distilled at 140°C under vacuum (10^{-2} torr) to yield a yellow oil containing a mixture of isomers, which was used without further purification (50% yield). A different preparation is described in ref. 6.

***ansa*-{[2,4-$(Me_3C)_2C_5H_2]_2SiMe_2$}Mg.** The tetraene [2,4-$(Me_3C)_2C_5H_3]_2SiMe_2$ (8.2 g, 20 mmol) was treated with dibutylmagnesium (26 mL, 0.76 M, 20 mmol) in heptane. The mixture was heated to vigorous reflux with stirring for 7 days, after which time the solvent was removed under dynamic vacuum, leaving a colourless solid, which was used without purification because it was clean by ^{1}H NMR spectroscopy (4.95 g, 54%). mp 125-126°C. ^{1}H NMR (C_6D_6): δ 6.58 (s, 4H, C_5H_2), 1.25 (s, 36H, Me_3C), -0.01 (s, 6H, Me_2Si).

***ansa*-{[$(Me_3Si)_2C_5H_2]_2SiMe_2$}Mg.** This complex was prepared in a similar manner to that used for the Me_3C analogue and isolated in 51 % yield. ^{1}H NMR (C_6D_6): δ 6.83 (s, 4H, C_5H_2), 0.24 (s, 6H, Me_2Si), -0.04 (s, 36H, Me_3Si).

***ansa*-{[2,4-$(Me_3C)_2C_5H_2]_2SiMe_2$}Fe.** Tetrahydrofuran (200 mL) was added to a mixture of $FeBr_2(THF)_2$ (4.09 g, 11.4 mmol) and *ansa*-{[2,4-$(Me_3C)_2C_5H_2]_2SiMe_2$}Mg (4.95 g, 11.4 mmol). The solution turned dark reddish-brown immediately and over the next 48 h became dark red. The solvent was removed under reduced pressure and the solid was extracted with hexane (200 mL) and filtered. The dark red filtrate was concentrated to a volume of 10 mL and cooled slowly to -40°C. Large red crystals formed (1.50 g, 28%). mp 140-142°C. Anal. Calcd for $C_{28}H_{46}FeSi$: C, 72.08; H, 9.94. Found: C, 71.79; H, 9.80. ^{1}H NMR (C_6D_6): δ 4.31 (s, 2H, C_5H_2), 4.28 (s, 2H, C_5H_2), 1.30 (s, 36H, Me_3C), 0.67 (s, 6H, Me_2Si) ppm. The E.I. mass spectrum showed a parent ion at m/e= 466 emu. The parent ion isotopic cluster was simulated: (calcd %, obsvd. %): 464 (6, 6), 465 (2, 3), 466 (100, 100), 467 (39, 36), 468 (11, 10), 469 (2, 2).

***ansa*-{[3,4-$(Me_3Si)_2C_5H_2]_2SiMe_2$}Fe.** This complex was prepared in a manner similar to that used for the preparation of the Me_3C analogue. Large, extremely soluble red-violet crystals were isolated by cooling a saturated hexane solution to -40 °C (10%). mp 203-205°C. Anal. Calcd for $C_{22}H_{46}FeSi_5$: C, 54.3; H, 8.78. Found: C, 52.8; H, 8.66. ^{1}H NMR (C_6D_6): δ 4.42 (m, 4H, C_5H_2), 0.35 (s, 36H, Me_3Si), 0.47 (s, 6H, Me_2Si) ppm.

[2,4-$(Me_3C)_2C_5H_2]_2SiMe_2Na_2$. Sodium amide (0.72 g, 18.5 mmol) was transferred to a large Schlenk tube equipped with a magnetic stirrer and suspended in THF (60 mL). The tetraene [2,4-$(Me_3C)_2C_5H_3]_2SiMe_2$ (3.45 g, 8.4 mmol) was weighed into a Schlenk flask and dissolved in THF (50 mL). The solution of [2,4-$(Me_3C)_2C_5H_3]_2SiMe_2$ was added to the suspension of $NaNH_2$ with stirring. The yellowish suspension was stirred at room temperature overnight. The contents of the Schlenk tube were transferred to a centrifuge bottle which was centrifuged at 3000 rpm for 30 minutes. The clear yellow solution was decanted into a clean flask. The solvent was removed under reduced pressure and the residue was washed in pentane. The base-free disodium salt was obtained by prolonged exposure (24 hours) of powdered samples to dynamic vacuum at room temperature.

***ansa*-{[2,4-$(Me_3C)_2C_5H_2]_2SiMe_2$}Yb(OEt_2).** The base-free disodium salt [2,4-$(Me_3C)_2C_5H_2]_2SiMe_2Na_2$ (2.3 g, 4.4 mmol) was stirred with a suspension of YbI_2 (2.0 g, 4.7 mmol) in diethyl ether overnight. Pale green crystals were isolated after filtration, concentration, and cooling of the solution to -40°C (2.5g, 86%). mp 275-282°C. Anal. Calcd for $C_{32}H_{56}OSiYb$: C, 58.4; H, 8.58. Found: C, 58.4; H, 8.67. ^{1}H NMR (C_6D_6): δ 6.26

(d, J = 2.6 Hz, 2H, C_5H_2), 5.99 (d, J = 2.6 Hz, 2H, C_5H_2), 3.02 (br q, 4H, OEt_2), 1.51 (s, 18H, Me_3C), 1.23 (s, 6H, $SiMe_2$), 1.22 (s, 18H, Me_3C), 0.96 (t, J = 7 Hz, 6H, OEt_2) ppm.

***ansa*-{[2,4-$(Me_3C)_2C_5H_2]_2SiMe_2$}Yb(THF)$_2$.** The green etherate *ansa*-{[2,4-$(Me_3C)_2C_5H_2]_2SiMe_2$}Yb(OEt_2) was dissolved in THF resulting in an immediate colour-change to deep purple. The solvent was removed under reduced pressure and the resulting pink residue was extracted into diethyl ether and cooled. Red crystals were obtained in 50% yield by cooling to -40°C. The low yield presumably reflects the high solubility of the product rather than any side reactions. mp 248-255°C. Anal. Calcd for $C_{36}H_{62}O_2SiYb$: C, 59.4; H, 8.58. Found: C, 59.5; H, 8.48. ^{1}H NMR (C_6D_6): δ 6.26 (d, J = 2.4 Hz, 2H, C_5H_2), 5.97 (d, J = 2.4 Hz, 2H, C_5H_2), 3.42 (br m, 8H, THF), 1.54 (s, 18H, Me_3C), 1.28 (m, 8H, THF), 1.22 (s, 6H, Me_2Si), 1.20 (s, 18H, Me_3C) ppm.

***ansa*-{[2,4-$(Me_3C)_2C_5H_2]_2SiMe_2$}Yb(2,6-$Me_2C_6H_3NC)_2$.** The isocyanide 2,6-$Me_2C_6H_3NC$ (0.18 g, 14.4 mmol) was added under a flow of nitrogen to a Schlenk flask containing *ansa*-{[2,4-$(Me_3C)_2C_5H_2]_2SiMe_2$}Yb(OEt_2) (0.5 g, 7.7 mmol). Toluene (25 mL) was added and the dark red solution was stirred briefly. The volume of solvent was reduced slightly and the solution was cooled to -40°C, resulting in the formation of dark red crystals in good yield. mp 245-247°C. Anal. Calcd for $C_{46}H_{64}N_2SiYb$: C, 65.3; H, 7.62; N, 3.31. Found C, 64.3; H, 8.03; N, 3.17. ^{1}H NMR (C_6D_6): δ 6.80 (t, J = 7.5 Hz, 2H, C_6H_3), 6.51 (d, J = 2.5 Hz, 2H, C_5H_2), 6.49 (d, J = 7.5 Hz, 4H, C_6H_3), 6.36 (d, J = 2.5 Hz, 2H, C_5H_2), 2.09 (s, 12H, $\underline{Me}_2C_6H_3$), 1.67 (s, 18H, Me_3C), 1.56 (s, 18H, Me_3C), 1.31 (s, 6H, Me_2Si) ppm.

Crystallographic Studies

A crystal of appropriate dimensions was mounted on a glass fibre using Paratone N hydrocarbon oil. All measurements were made on a Bruker SMART 1K CCD diffractometer.[40] Cell constants and an orientation matrix were obtained of the measured positions of reflections with I > 10 σ to give the unit cell. The systematic absences uniquely determined the space group in each case. An arbitrary hemisphere of data was collected at low temperature (see Tables 2 and 4 for details) using the ω scan technique with 0.3° scans counted for 10-30 s per frame. Data were integrated using SAINT[41] and corrected for Lorentz and polarisation effects. The data were analysed for agreement and absorption using XPREP,[42] and an empirical absorption correction was applied based on comparison of redundant and equivalent reflections. The structures were solved by direct methods and expanded using Fourier techniques. Non-hydrogen atoms were refined anisotropically (unless stated otherwise), and the hydrogen atoms were included in calculated positions, but not refined. The ytterbium structures were solved and refined using the software package TeXsan,[43] in all other cases SHELXS-97 (structure solution)[44] and SHELXL-97 (refinement)[45] were used. The structure solution refinements were unexceptional, except for the following two compounds.

***ansa*-{[2,4-$(Me_3C)_2C_5H_2]_2SiMe_2$}Yb(OEt_2).** Only Friedel-equivalent (P222) data were merged. Five of the carbon atoms were refined isotropically while the remainder of the non-hydrogen atoms were refined anisotropically. The absolute configuration analysis performed by teXsan indicated that the enantiomorph was correct, and it has a lower R factor than the inverted structure. A diffuse region of electron density in the structure which is possibly disordered solvent has been modelled as 24 partial occupancy carbon atoms. The initial positions of these atoms was based on the largest peaks in the difference Fourier map, and subsequent refinement and examination of the Fourier and difference Fourier maps indicated that the electron density is centred around those positions. The thermal parameters of these carbon atoms was fixed at 8.0 and their individual occupancy parameters were refined. Refinement led to occupancies of between 0.195 and 0.710. The sum of the occupancies is 9.855 which is approximately equal to one and a third diethyl ether molecules per asymmetric unit.

***ansa*-{[2,4-$(Me_3C)_2C_5H_2]_2SiMe_2$}Yb(2,6-$Me_2C_6H_3NC)_2$.** Due to poor data, one cyclopentadienide ring carbon atom was refined isotropically while the remainder of the non-hydrogen atoms were refined anisotropically with the following exception: one of the Me_3C groups on one of the cyclopentadienide rings was disordered. It was modelled with two sets of three methyl groups, each set having their occupancies constrained to be equal, and the sum of the occupancies of the two sets constrained to 1.0. Refinement led to occupancies of 0.49 and 0.51 for the sets of methyl carbon atoms. These atoms were refined isotropically.

Acknowledgments

This work was supported by the Director, Office of Energy Research, Office of Basic Energy Sciences, Chemical Sciences Division of the U.S. Department of Energy under Contract No. DE-AC03-76SF00098. We thank Dr Fred Hollander (at CHEXRAY, the U. C. Berkeley X-ray diffraction facility) for assistance with the crystallography. We are grateful to Ged Parkin for providing reference 14 in advance of publication.

Supporting Information

Crystallographic data for the structures reported in this paper have been deposited with the Cambridge Crystallographic Data Centre. Copies of the data (CCDC 245770-245775) can be obtained free of charge via www.ccdc.cam.ac.uk/data_request/cif, by emailing data_request@ccdc.cam.ac.uk, or by contacting The Cambridge Crystallographic Data Centre, 12, Union Road, Cambridge CB2 1EZ, UK; fax: +44 1223 336033.

References

1. H. H. Brintzinger, D. Fischer, R. Mülhaupt, B. Rieger and R. M. Waymouth, *Angew. Chem., Int. Ed. Engl.*, 1995, **34**, 1143-1170.
2. W. Kaminsky, Metalorganic Catalysts for Synthesis and Polymerization, Springer Verlag, Berlin, 1999.
3. A. Togni and R. L. Halterman, Metallocenes, Wiley, Weinheim, 1998.
4. H. Schumann, J. A. Meese-Marktscheffel and L. Esser, *Chem. Rev.*, 1995, **95**, 865-986.
5. M. Douglass, M. Ogasawara, S. Hong, M. V. Metz and T. J. Marks, *Organometallics*, 2002, **21**, 283-292 and references therein.
6. E. Ihara, M. Nodono, K. Katsura, Y. Adachi, H. Yasuda, M. Yamagashira, H. Hashimoto, N. Kanehisa and Y. Kai, *Organometallics*, 1998, **17**, 3945-3956.
7. P. B. Hitchcock, M. F. Lappert and S. Tian, *Organometallics*, 2000, **19**, 3420-3428.
8. S. J. Swamy, J. Loebel and H. Schumann, *J. Organomet. Chem.*, 1989, **379**, 51-58.
9. M. Schultz, C. J. Burns, D. J. Schwartz and R. A. Andersen, *Organometallics*, 2001, **20**, 5690-5699.
10. P. Selg, H. H. Brintzinger, M. Schultz and R. A. Andersen, *Organometallics*, 2002, **21**, 3100-3107.
11. L. Maron, L. Perrin, O. Eisenstein and R. A. Andersen, *J. Am. Chem. Soc.*, 2002, **124**, 5614-5615.
12. L. Perrin, L. Maron, O. Eisenstein, D. J. Schwartz, C. J. Burns and R. A. Andersen, *Organometallics*, 2003, **22**, 5447-5453.
13. C. E. Zachmanoglou, A. Docrat, B. M. Bridgewater, G. Parkin, C. J. Brandow, J. E. Bercaw, C. N. Jardine, M. Lyall, J. C. Green and J. B. Keister, *J. Am. Chem. Soc.*, 2002, **124**, 9525-9546.
14. G. Parkin, personal communication, 2004.
15. P. Jutzi, *Chem. Rev.*, 1986, **86**, 983-996.
16. M. Schultz, C. J. Burns, D. J. Schwartz and R. A. Andersen, *Organometallics*, 2000, **19**, 781-789.
17. P. L. Watson, Structure of $(Me_5C_5)_2Yb(OEt_2)$, personal communication, 1981. Selected data: $C_{24}H_{40}OYb$, FW = 517.61,

orthorhombic, $P2_12_12_1$ (#19), T = 173K, a = 15.100(2) Å, b = 18.289(2) Å, c = 8.540(1) Å, V = 2358 Å^3, Z = 4, d_{calc} = 1.458 g/cm^3, 2274 reflections, 253 variables, R = 0.028.

18. A. V. Khvostov, A. I. Sizov, B. M. Bulychev, S. Y. Knjazhanski and V. K. Belsky, *J. Organomet. Chem.*, 1998, **559**, 97-105.
19. R. D. Rogers, *J. Organomet. Chem.*, 1996, **512**, 97-100.
20. L. Pauling, The Nature of the Chemical Bond, Cornell University Press, Ithaca, NY, 1960, pp 260 and 403.
21. T. D. Tilley, R. A. Andersen, B. Spencer, H. Ruben, A. Zalkin and D. H. Templeton, *Inorg. Chem.*, 1980, **19**, 2999-3003.
22. T. D. Tilley, R. A. Andersen, B. Spencer and A. Zalkin, *Inorg. Chem.*, 1982, **21**, 2647-2649.
23. C. J. Burns and R. A. Andersen, *J. Am. Chem. Soc.*, 1987, **109**, 915-917.
24. C. J. Burns and R. A. Andersen, *J. Am. Chem. Soc.*, 1987, **109**, 941-942.
25. C. J. Burns and R. A. Andersen, *J. Am. Chem. Soc.*, 1987, **109**, 5853-5855.
26. P. B. Hitchcock, J. A. K. Howard, M. F. Lappert and S. Prashar, *J. Organomet. Chem.*, 1992, **437**, 177-189.
27. J. C. Green, D. Hohl and N. Rösch, *Organometallics*, 1987, **6**, 712-720.
28. M. Gerloch and E. C. Constable, Transition Metal Chemistry, VCH, Weinheim, 1995, Chapter 10.
29. R. E. Da Re, C. J. Kuehl, M. G. Brown, R. C. Rocha, E. D. Bauer, K. D. John, D. E. Morris, A. P. Shreve and J. L. Sarrao, *Inorg. Chem.*, 2003, **42**, 5551-5559.
30. H. Schumann, M. Glanz, H. Hemling and F. E. Hahn, *Z. Anorg. Allg. Chem.*, 1995, **621**, 341-345.
31. M. F. Lappert, P. I. W. Yarrow, J. L. Atwood, R. Shakir and J. Holton, *J. Chem. Soc., Chem. Commun.*, 1980, 987-988.
32. Q. Shen, D. Zheng, L. Lin and Y. Lin, *J. Organomet. Chem.*, 1990, **391**, 321-326.
33. A. W. Duff, P. B. Hitchcock, M. F. Lappert and R. G. Taylor, *J. Organomet. Chem.*, 1985, **293**, 271-283.
34. C. D. Sofield and R. A. Andersen, *J. Organomet. Chem.*, 1995, **501**, 271-276.
35. W. W. Lukens, S. M. Beshouri, L. L. Blosch, A. C. Stuart and R. A. Andersen, *Organometallics*, 1999, **18**, 1235-1246.
36. A. J. Leffler, *Inorg. Chem.*, 1968, **7**, 2651-2652.
37. K. W. Greenlee and A. L. Henne, *Inorg. Synth.*, 1946, **2**, 128-135.
38. T. D. Tilley, J. M. Boncella, D. J. Berg, C. J. Burns and R. A. Andersen, *Inorg. Synth.*, 1990, **27**, 146-149.
39. J. M. Boncella, PhD Thesis, University of California, Berkeley, 1984.
40. *SMART Area-Detection Software Package*; Siemens Industrial Automation, Inc, Madison, WI, 1995.
41. *SAINT*, 4.024; Siemens Industrial Automation, Inc, Madison, WI, 1995.
42. G. M. Sheldrick. *XPREP*, 5.03; Siemens Industrial Automation, Inc, Madison, WI, 1995.
43. *teXsan Crystal Structure Analysis Package*; Molecular Structure Corporation, Inc, The Woodlands, TX, 1992.
44. G. M. Sheldrick. *SHELXS-97*; University of Göttingen, Germany, 1997.
45. G. M. Sheldrick. *SHELXL-97*; University of Göttingen, Germany, 1997.

Table 1. Selected bond distances (Å) and bond angles (°) of *ansa*-ferrocenes

	ansa-{[3,4-$(Me_3Si)_2C_5H_2]_2SiMe_2$}Fe	*ansa*-{[2,4-$(Me_3C)_2C_5H_2]_2SiMe_2$}Fe
Fe - C (mean)	2.07	2.06
Fe - C (range)	2.027(3) - 2.129(3)	2.015(2) - 2.097(2)
Fe - centroid	1.67	1.66
centroid - Fe - centroid	160.5	165.5
C(ring) - Si - C(ring)	92.8(1)	96.7(1)
α	26.3(2)	20.3(1)
β	56.7(1)	52.1(1)
γ	92.8(1)	96.7(1)
δ	160.5	165.5

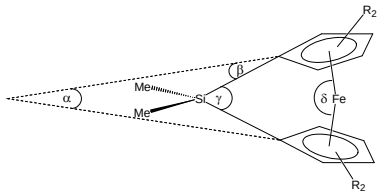

Figure for Table 1

Table 2. Selected data collection and structure solution parameters for *ansa*-ferrocenes and $[2,4\text{-}(Me_3C)_2C_5H_3]SiMe_2$

compound	*ansa*-{[3,4-$(Me_3Si)_2C_5H_2]_2SiMe_2$}Fe	$[2,4\text{-}(Me_3C)_2C_5H_3]_2SiMe_2$	*ansa*-{[2,4-$(Me_3C)_2C_5H_2]_2SiMe_2$}Fe
formula	$C_{24}H_{46}FeSi_5$	$C_{28}H_{48}Si$	$C_{28}H_{46}FeSi$
FW	530.91	412.75	466.59
space group	C2/c (#15)	$P2_1/c$ (#14)	C2/c (#15)
a (Å)	15.507(1)	9.123(1)	31.016(1)
b (Å)	12.067(1)	16.806(1)	9.907(1)
c (Å)	32.668(1)	18.725(1)	19.618(1)
β(°)	96.810(1)	76.758(1)	117.403(1)
V ($Å^3$)	6070.09(9)	2794.68(7)	5351.4(1)
Z	8	4	8
d_{calc} (g/cm^3)	1.162	0.981	1.158
μ(Mo-Kα)$_{calc}$	0.70 mm^{-1}	0.09 mm^{-1}	0.62 mm^{-1}
size (mm)	0.32 × 0.28 × 0.18	0.39 × 0.33 × 0.13	0.33 × 0.28 × 0.28
temperature (K)	159	176	98
scan type, range	ω, 4 – 45°	ω, 6 – 46.5°	ω, 4 – 52.2°
reflections integrated	12365	11363	12202
unique reflections, R_{int}	4353 (0.040)	3985, 0.031	4722, 0.030
good reflections	3812 $F_o^2>2\sigma(F_o^2)$	3501 $F_o^2>2\sigma(F_o^2)$	4180 $F_o^2>2\sigma(F_o^2)$
variables	285	276	285
transmission range	0.884 - 0.801	0.988 - 0.820	0.8454 - 0.8214
R	0.042	0.0464	0.042
R_w	0.098	0.1139	0.105
R_{all}	0.052	0.0540	0.049
GOF	1.169	1.089	1.02
max/min peaks in final difference map	0.34/-0.23 $e^-/Å^3$	0.30/-0.22 $e^-/Å^3$	0.76/-0.45 $e^-/Å^3$

Table 3. Selected bond distances (Å) and bond angles (°) of the diethyl ether adducts $Cp'_2Yb(OEt_2)$ and *ansa*-ytterbocene isocyande complex

	ansa-{[2,4-$(Me_3C)_2C_5H_2]_2SiMe_2$}Yb(OEt_2)	[1,3-$(Me_3C)_2C_5H_3]_2$Yb(OEt_2)	$(Me_5C_5)_2$Yb(OEt_2) [a]	*ansa*-{[2,4-$(Me_3C)_2C_5H_2]_2SiMe_2$}Yb($CNC_8H_9)_2$
M - C (mean)	2.71	2.71	2.69	2.71
M - C (range)	2.61(1) - 2.80(1)	2.651(6) - 2.765(6)	2.66(1) - 2.729(7)	2.63(1) - 2.81(1)
M - centroid	2.43	2.44	2.41	2.43
M - O (CN)	2.44(1); 2.411(9); 2.36(1)	2.442(4)	2.467(7)	2.57
Cp(centroid) - Yb - Cp(centroid)	123.8	131.8	140.6	123.1
C(ring) - Si - C(ring)	103.2(7)			103.4(5)
intramolecular contact	3.14(1); 3.15(1); 3.00(1)	none	3.23(1)	

a From ref. 17.

Data for unique molecules in the asymmetric unit presented as Yb(1); Yb(2); Yb(3).

Table 4. Selected data collection and structure solution parameters for diethyl ether adducts $Cp'_2Yb(OEt_2)$ and *ansa*-{[2,4-$(Me_3C)_2C_5H_2]_2SiMe_2$}Yb(2,6-$Me_2C_6H_3NC)_2$

compound	*ansa*-{[2,4-$(Me_3C)_2C_5H_2]_2$ $SiMe_2$}Yb(OEt_2)	[1,3-$(Me_3C)_2C_5H_3]_2$Yb(OEt_2)	*ansa*-{[2,4-$(Me_3C)_2C_5H_2]_2$ $SiMe_2$}Yb(2,6-$Me_2C_6H_3NC)_2$
formula	$YbSiC_{32}H_{56}O$	$YbC_{30}H_{52}O$	$YbSiN_2C_{46}H_{64}$
FW	657.92	601.78	846.15
space group	$P2_12_12_1$ (#19)	$P2_1/n$ (#14)	$P2_1/n$ (#14)
a (Å)	29.0586(5)	11.1771(2)	11.8426(6)
b (Å)	15.9398(2)	19.1123(1)	16.4380(9)
c (Å)	24.5206(4)	14.0739(2)	22.338(1)
β(°)		90.160(1)	99.068(1)
V ($Å^3$)	11357.7(3)	3006.47(8)	4294.1(3)
Z	12	4	4
d_{calc} (g/cm^3)	1.154	1.329	1.309
μ(Mo-Kα)$_{calc}$	25.19 cm^{-1}	31.28 cm^{-1}	22.37 cm^{-1}
size (mm)	0.60 × 0.10 × 0.08	0.26 × 0.25 × 0.15	0.36 × 0.11 × 0.08
temperature (K)	156	131	163
scan type, range	ω, 4 - 46.6°	ω, 4 - 52.2°	ω, 4 - 52.3°
reflections integrated	47621	14404	17261
unique reflections, R_{int}	16331, 0.070	5451, 0.045	6369, 0.083
good reflections	9671 $F_o^2>3\sigma(F_o^2)$	3667 $F_o^2>3\sigma(F_o^2)$	3243 $F_o^2>3\sigma(F_o^2)$
variables	1017	289	444
transmission range	0.928 - 0.787	0.989 - 0.796	0.977 - 0.626
R	0.046	0.033	0.045
R_w	0.047	0.039	0.051
R_{all}	0.088	0.045	0.102
GOF	1.24	1.29	1.18
max/min peaks in final difference map	2.12/-1.23 $e^-/Å^3$	1.52/-0.71 $e^-/Å^3$	1.20/-1.42 $e^-/Å^3$

Table 5. Optical spectra of ytterbocene etherates and the isocyanide complex *ansa*-{[2,4-$(Me_3C)_2C_5H_2]_2SiMe_2$}Yb(2,6-$Me_2C_6H_3NC)_2$ (in methylcyclohexane unless specified)

Compound	λ_{max} in nm (ε in $Lmol^{-1}cm^{-1}$)
ansa-{[2,4-$(Me_3C)_2C_5H_2]_2SiMe_2$}Yb(OEt_2)	664 (199), 460 (410), 399 (552)
ansa-{[2,4-$(Me_3C)_2C_5H_2]_2SiMe_2$}Yb($THF)_2$	676 (152), 490 (376), 378 (497)
ansa-{[2,4-$(Me_3C)_2C_5H_2]_2SiMe_2$}Yb($THF)_2$ in toluene	670 (142), 484 (351), 375 (453)
$(Me_5C_5)_2$Yb(OEt_2)	690 (216), 472 (356), 407 (435)
$(Me_5C_5)_2$Yb(OEt_2) in toluene	686 (251), 449 (429), 393 (537)
$(Me_5C_5)_2$Yb($THF)_2$	800 (266), 513 (437), 448 (533)
$(Me_5C_5)_2$Yb(THF)	801 (217), 513 (355), 447 (450)
$[1,3\text{-}(Me_3C)_2C_5H_3]_2$Yb($OEt_2$)	655 (211), 455 (480), 397 (486)
$[1,3\text{-}(Me_3C)_2C_5H_3]_2$Yb(THF)	654 (188), 477 (395), 387 (366)
$[1,3\text{-}(Me_3C)_2C_5H_3]_2$Yb(THF) in THF	641 (190), 467 (400), 386 (400)
$[1,3\text{-}(Me_3Si)_2C_5H_3]_2$Yb($OEt_2$)	653 (216), 477 (333), 392 (466)
$[1,3\text{-}(Me_3Si)_2C_5H_3]_2$Yb(THF)	678 (161), 494 (252), 399 (292)
$(Me_4C_5H)_2$Yb(OEt_2)	683 (186), 468 (294), 401 (382)
$(Me_4C_5H)_2$Yb($THF)_2$	785 (107), 514 (230), 439 (280)
$(Me_4C_5H)_2$Yb(THF)	780 (146), 511 (286), 440 (353)
ansa-{[2,4-$(Me_3C)_2C_5H_2]_2SiMe_2$}Yb(2,6-$Me_2C_6H_3NC)_2$ in toluene	686 (500), 500 (613)

Figure captions

Figure 1. ORTEP diagram of *ansa*-{[3,4-$(Me_3Si)_2C_5H_2]_2SiMe_2$}Fe (50% probability ellipsoids).

Figure 2. ORTEP diagram of $[2,4\text{-}(Me_3C)_2C_5H_3]_2SiMe_2$ (50% probability ellipsoids). Selected distances (Å) and angles (°): C1 – Si1 1.928(2); C14 – Si1 1.925(2); C27 – Si1 1.871(2); C28 – Si1 1.878(2); C1 – Si1 – C14 105.24(8); C27 – Si1 – C28 113.0(1); C1 – Si1 – C27 113.4(1).

Figure 3. ORTEP diagram of *ansa*-{[2,4-$(Me_3C)_2C_5H_2]_2SiMe_2$}Fe (50% probability ellipsoids).

Figure 4. ORTEP diagram of *ansa*-{[2,4-$(Me_3C)_2C_5H_2]_2SiMe_2$}Yb(OEt_2) (50% probability ellipsoids) (only one of three unique molecules shown).

Figure 5. ORTEP diagram of $[1,3\text{-}(Me_3C)_2C_5H_3]_2$Yb($OEt_2$) (50% probability ellipsoids).

Figure 6. ORTEP diagram of *ansa*-{[2,4-$(Me_3C)_2C_5H_2]_2SiMe_2$}Yb(2,6-$Me_2C_6H_3NC)_2$ (only one of disordered Me_3C groups shown) (50% probability ellipsoids). Selected bond distances (Å) and angles (°) not given in Table 3: C_{CNR} - N 1.15; N - CR 1.44; C_{CNR} - Yb - C_{CNR} 78.5(4); Yb - C_{CNR} - N 172.5; C_{CNR} - N - CR 178.0.

Figure 7. Schematic energy diagram showing the possible effects of an additional ligand on the energies of the molecular orbitals and the HOMO → LUMO transition of a bent metallocene.

Figure 8. Optical spectra of diethyl ether adducts of ytterbocenes in methylcyclohexane.

Figure 9. Optical spectra of THF adducts of ytterbocenes in methylcyclohexane.

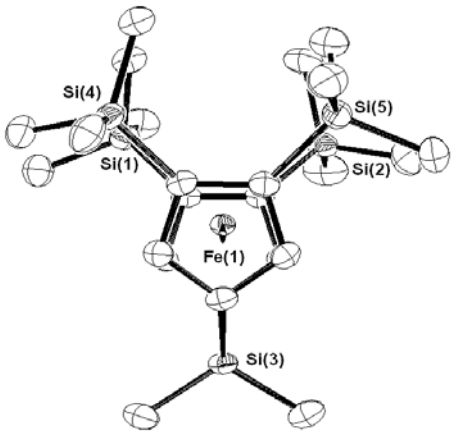

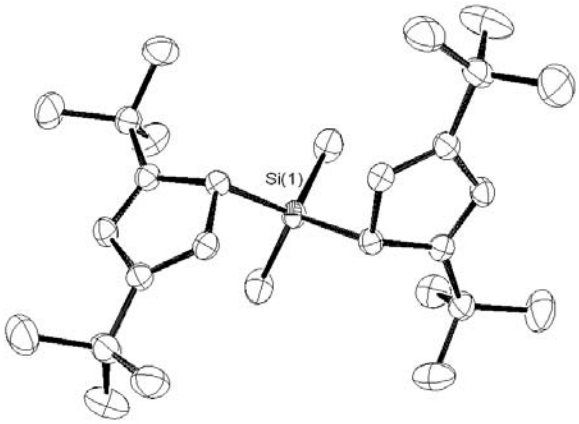

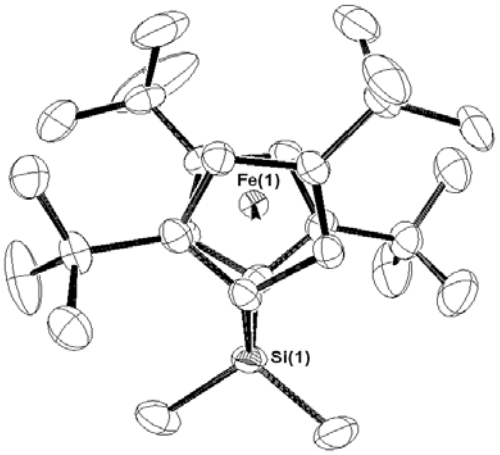

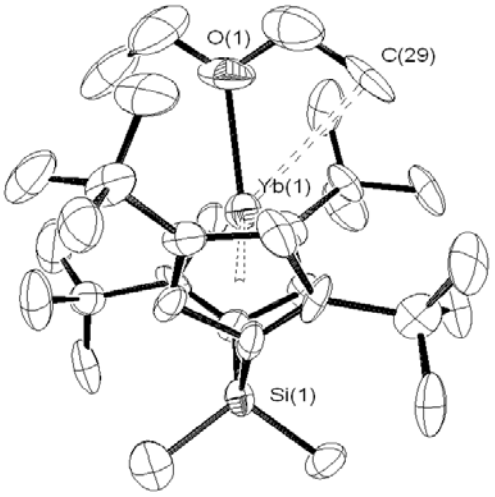
O(1)
C(29)
Yb(1)
Si(1)

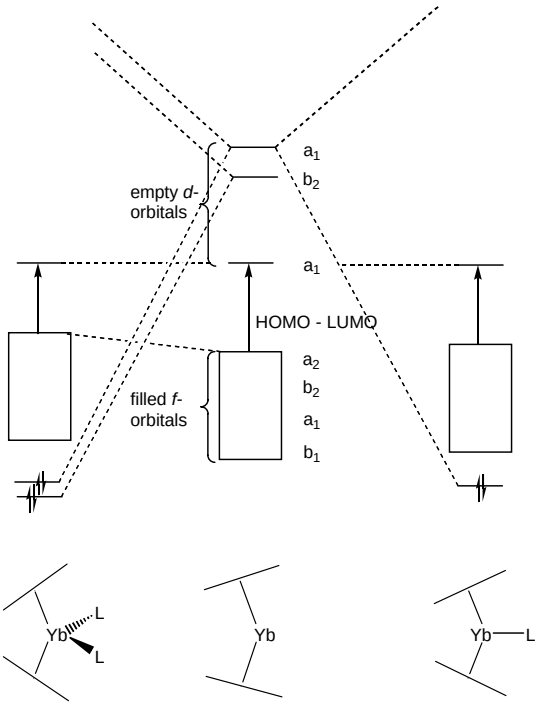
a1
b2
empty d-orbitals
a1
HOMO - LUMO
a2
b2
filled f-orbitals
a1
b1
Yb
L
L
Yb
Yb
L

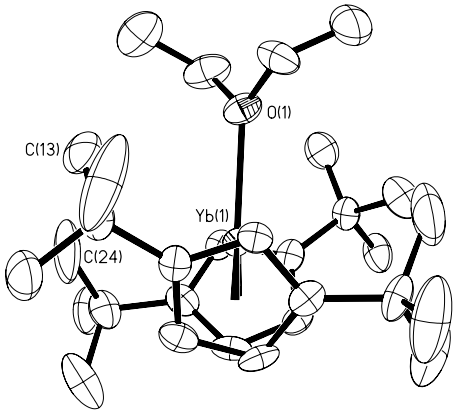
O(1)
C(13)
Yb(1)
C(24)

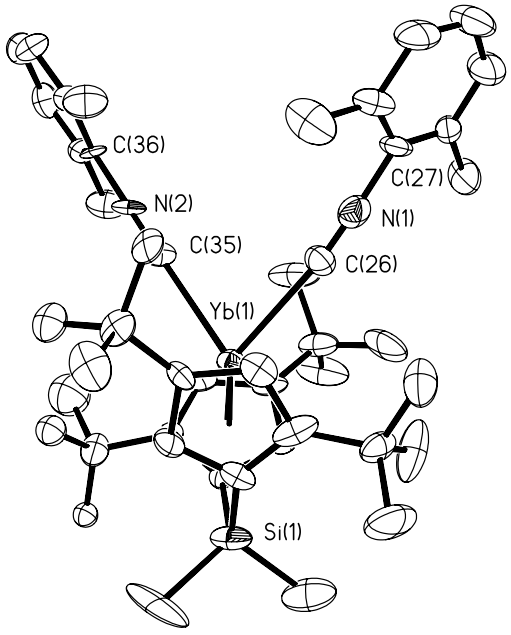
C(36)
N(2)
C(35)
Yb(1)
C(27)
N(1)
C(26)
Si(1)

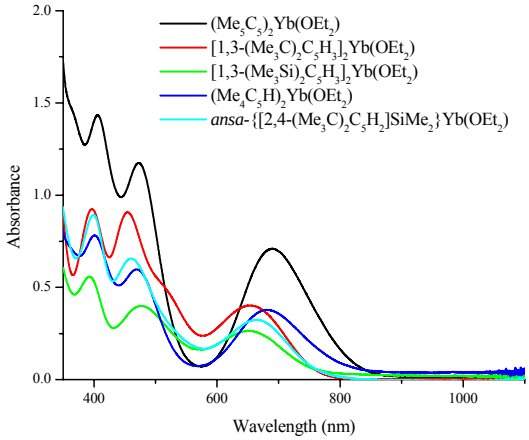
(Me5C5)2Yb(OEt2)
[1,3-(Me3C)2C5H3]2Yb(OEt2)
[1,3-(Me3Si)2C5H3]2Yb(OEt2)
(Me4C5H)2Yb(OEt2)
ansa-{[2,4-(Me3C)2C5H2]SiMe2}Yb(OEt2)
Absorbance
Wavelength (nm)

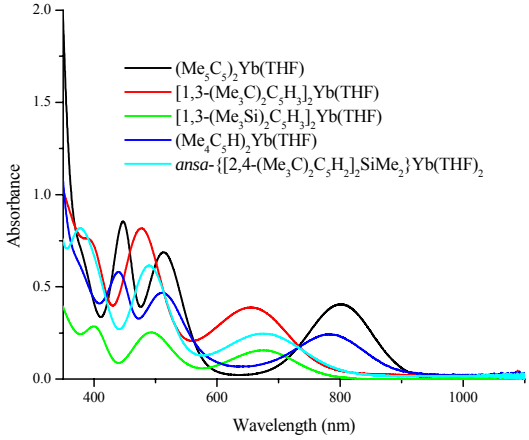
(Me5C5)2Yb(THF)
[1,3-(Me3C)2C5H3]2Yb(THF)
[1,3-(Me3Si)2C5H3]2Yb(THF)
(Me4C5H)2Yb(THF)
ansa-{[2,4-(Me3C)2C5H2]2SiMe2}Yb(THF)2
Absorbance
Wavelength (nm)